Dynamical Magnetic Field Accompanying the Motion of Ferroelectric Domain Walls

Dominik M. Juraschek,[1,*,†] Quintin N. Meier,[1] Morgan Trassin,[1] Susan E. Trolier-McKinstry,[2] Christian L. Degen,[3] and Nicola A. Spaldin[1]

[1]*Department of Materials, ETH Zurich, CH-8093 Zürich, Switzerland*

[2]*Materials Science and Engineering Department and Materials Research Institute, The Pennsylvania State University, University Park, Pennsylvania 16802, USA*

[3]*Department of Physics, ETH Zurich, CH-8093 Zürich, Switzerland*

(Received 25 April 2019; published 17 September 2019)

The recently proposed dynamical multiferroic effect describes the generation of magnetization from temporally varying electric polarization. Here, we show that the effect can lead to a magnetic field at moving ferroelectric domain walls, where the rearrangement of ions corresponds to a rotation of ferroelectric polarization in time. We develop an expression for the dynamical magnetic field, and calculate the relevant parameters for the example of 90° and 180° domain walls, as well as for polar skyrmions, in $BaTiO_3$, using a combination of density functional theory and phenomenological modeling. We find that the magnetic field reaches the order of several μT at the center of the wall, and we propose two experiments to measure the effect with nitrogen-vacancy center magnetometry.

DOI: 10.1103/PhysRevLett.123.127601

The domain walls that separate different orientations of electric polarization in ferroelectric materials have long been of interest because their motion governs the process of ferroelectric switching in an electric field [1]. Recently, a range of unexpected behaviors has been discovered at domain walls that do not occur in the bulk of the domains, suggesting additional interest in domain walls as functional entities in their own right [2]. These include electrical conductivity [3–7] or even superconductivity [8] in otherwise insulating systems, ferrielectricity [9], as well as magnetoelectricity [10–14], strongly anisotropic magnetoresistance [15], and intriguing dualities between domain walls and the domains themselves [16].

Of particular interest for this work is the electric polarization that has been shown to arise at certain magnetic domain walls in otherwise nonpolar materials [17–20]. The local wall polarization is a consequence of the spatially varying magnetization at the magnetic domain wall, and is described by $\mathbf{P} \sim \mathbf{M} \times (\nabla_{\mathbf{r}} \times \mathbf{M})$ [21,22]. This mechanism is well established for the case of bulk multiferroics, in which a macroscopic ferroelectric polarization is generated via a spin spiral [23–26]. Here we describe the reciprocal effect, in which dynamical magnetization may arise at moving ferroelectric domain walls in otherwise nonmagnetic materials. This phenomenon has its origin in the recently described dynamical multiferroic effect [27], which describes magnetization generated from temporally varying electric polarization. The magnetization is given by $\mathbf{M} \sim \mathbf{P} \times \partial_t \mathbf{P}$ [28], and the mechanism has been proposed to lead to new behaviors, including a phonon Zeeman effect [27], exotic quantum criticality [29], and phonon orbital magnetism [30].

Here, we discuss the link between dynamical multiferroicity and ferroelectric domain wall functionality by showing theoretically that the motion of ferroelectric domain walls can be accompanied by a dynamical magnetic field. After extending the formalism of dynamical multiferroicity to the case of domain wall motion, we present numerical results for the prototypical ferroelectric barium titanate ($BaTiO_3$), based on first-principles calculations combined with phenomenological modeling using experimental parameters. Finally, we discuss the possibility of detecting the dynamical magnetic field experimentally using nitrogen-vacancy center magnetometry.

Theoretical formalism.—We begin by deriving an expression for the dynamical magnetic field at ferroelectric domain walls. Our derivation extends the recently developed microscopic theory for calculating the magnetic moments of optical phonons within the dynamical multiferroicity framework [27] to the case of moving ionic charges at ferroelectric domain walls. The input parameters in the expression that we obtain can be computed using density functional theory.

The ionic magnetic moment $\mathbf{m}$ of a unit cell is given by

$$\mathbf{m} = \sum_i \mathbf{m}_i = \sum_i \gamma_i \mathbf{L}_i, \tag{1}$$

where $\mathbf{m}_i$ and $\mathbf{L}_i$ are the magnetic moment and the angular momentum arising from the motion of ion i, and the sum runs over all ions in the unit cell. $\gamma_i = e\mathbf{Z}_i^*/(2\mathcal{M}_i)$ is the gyromagnetic ratio tensor of the ion given by the elementary charge e, the Born effective charge tensor $\mathbf{Z}_i^*$, and the atomic mass $\mathcal{M}_i$.

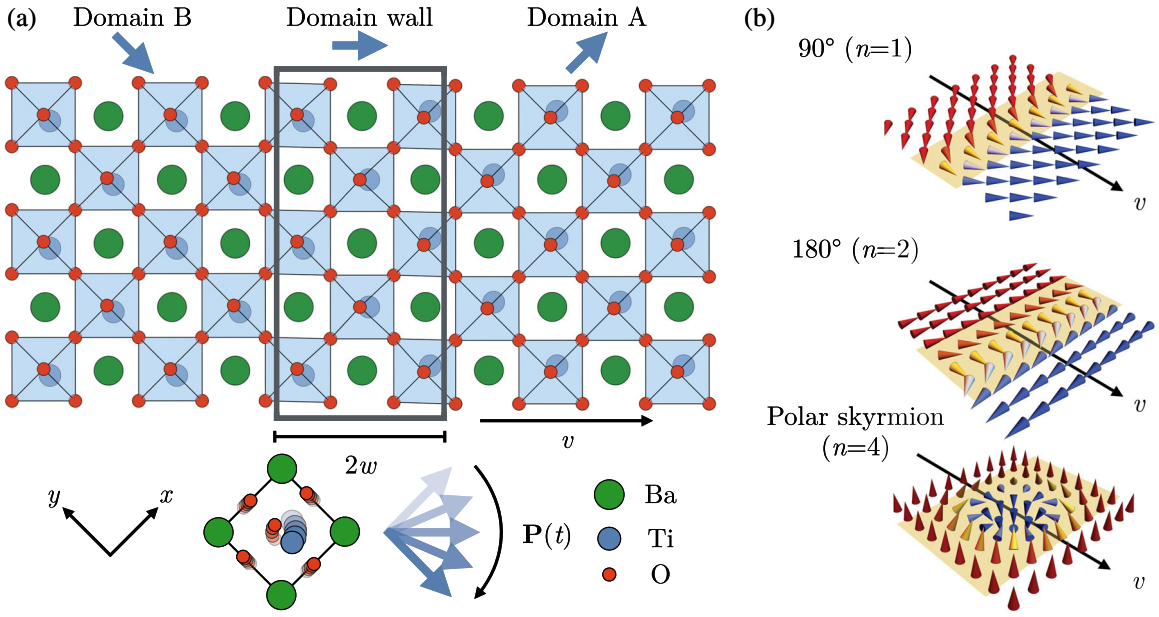

FIG. 1. (a) Schematic of a 90° domain wall in the xy plane of $BaTiO_3$ with thickness $2w$ and velocity v separating the two domains A and B. At the bottom, the rearrangement of the titanium and oxygen ions in the moving domain wall is depicted, as well as the change of ferroelectric polarization in time (thick arrows). The displacements of the oxygen and titanium ions are exaggerated for illustration purposes. Note that atomic radii, not ionic, are shown. (b) Illustration of the polarization evolution across 90° and 180° Néel-type domain walls, and in a polar skyrmion.

The angular momentum at a moving ferroelectric domain wall results from the rearrangement of the atomic positions of the ions in ferroelectric domain A to their respective positions in domain B, see the example of a 90° domain wall in Fig. 1(a). As the domain wall passes by, the ferroelectric displacement corresponding to domain A, $\mathbf{U}_{i,x}$, reduces to zero, while that corresponding to domain B, $\mathbf{U}_{i,y}$, increases to its bulk value. The angular momentum of ion i can then be written as

$$\mathbf{L}_i = \mathcal{M}_i(\mathbf{U}_{i,x} \times \partial_t \mathbf{U}_{i,y} + \mathbf{U}_{i,y} \times \partial_t \mathbf{U}_{i,x}). \tag{2}$$

We can write the time-dependent ferroelectric displacements in terms of a product of the bulk ferroelectric displacement vector $\mathbf{u}_{i,x}$ with a time-dependent dimensionless amplitude Q_x, $\mathbf{U}_{i,x}(t) = Q_x(t)\mathbf{u}_{i,x}$. The bulk ferroelectric displacement vector $\mathbf{u}_{i,x} = \mathbf{r}_{i,x} - \mathbf{r}_{i,\mathrm{HS}}$ is given by the difference between the atomic coordinates of the respective ferroelectric structure $\mathbf{r}_{i,x}$, and those of the corresponding high-symmetry structure $\mathbf{r}_{i,\mathrm{HS}}$. Inserting Eq. (2) into Eq. (1) we obtain

$$\mathbf{m} = \boldsymbol{\gamma}(\mathbf{Q} \times \partial_t \mathbf{Q})_z, \tag{3}$$

where $\mathbf{Q} = (Q_x, Q_y, 0)$ is the time-dependent dimensionless amplitude vector and the vector $\boldsymbol{\gamma} = \sum_i \gamma_i \mathcal{M}_i \mathbf{u}_{i,x} \times \mathbf{u}_{i,y}$ given in units of Asm^2 contains all atom-specific properties.

The time evolution of the rotation of polarization in a moving Néel-type ferroelectric domain wall, in which the ferroelectric polarization rotates within the surface plane, can be described by the sine-Gordon equation with the following solution:

$$\phi(r,t) = \arctan(e^{\beta(r-vt)/w}), \tag{4}$$

see, e.g., Refs. [31,32] and the Supplemental Material [33]. Here, ϕ is the rotation angle, r is the position perpendicular to the domain wall, v is the domain wall velocity, $2w$ is the width of the nonmoving domain wall, and the factor $\beta = 1/\sqrt{1 - v^2/c_0^2}$ describes a Lorentz-like contraction of the moving domain wall that becomes significant for velocities close to the characteristic velocity c_0 of the system [34], which corresponds to the transverse sound velocity [35,36]. Without loss of generality we set $r = 0$, and with $\phi(0,t) \equiv \phi(t)$ we model the time dependence of $\mathbf{Q}$ as

$$\mathbf{Q}(t) = \begin{pmatrix} Q_x(t) \\ Q_y(t) \end{pmatrix} = \begin{pmatrix} \cos(n\phi(t)) \\ \sin(n\phi(t)) \end{pmatrix}, \tag{5}$$

where n determines the amount of polarization rotation between the domains ($n = 1$ for a 90° domain wall).

Inserting Eqs. (4) and (5) into Eq. (3), the ionic magnetic moment per unit cell accompanying the motion of the domain wall reduces to

$$\mathbf{m}(t) = \boldsymbol{\gamma} n \partial_t \phi(t). \tag{6}$$

The internal magnetic field $\mathbf{B}$ created by the ionic magnetic moment of the moving domain wall is then given by

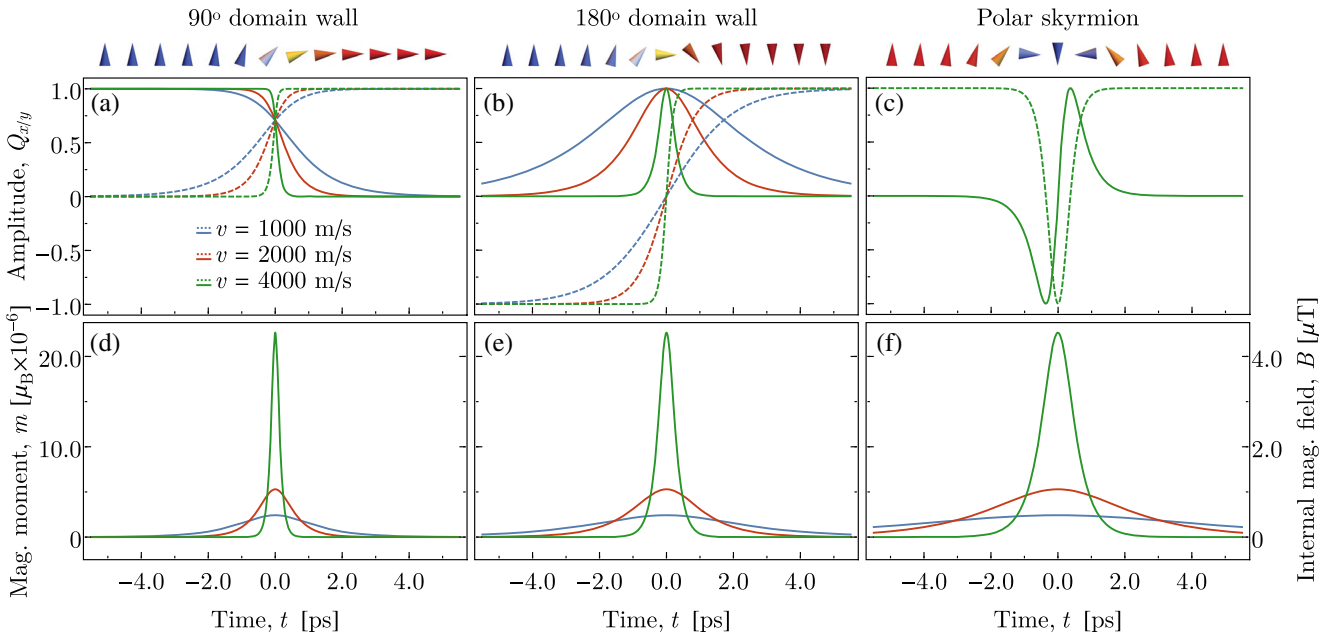

FIG. 2. Time evolution of domain walls. Shown are the dimensionless amplitudes Q_x (solid lines) and Q_y (dashed lines) for the (a) 90° domain wall, (b) 180° domain wall, and (c) polar skyrmion. In (c), the amplitudes are shown only for $v = 4000$ m/s for clarity. The resulting magnetic moments m in units of 10^{-6} μ_B and internal magnetic fields B in units of μT are shown in (d)–(f).

$\mathbf{B} = \mu_0 \mathbf{m}/V$, where μ_0 is the vacuum permeability and V the volume of the unit cell.

Numerical results.—We estimate the magnitude of the dynamical magnetic field according to Eq. (6) starting with the example of a 90° domain wall in $BaTiO_3$, see Fig. 1. The fundamental input parameters to Eq. (6) are the Born effective charge tensors $\mathbf{Z}_i^*$, the ferroelectric displacement vectors $\mathbf{u}_{i,x/y}$, and the volume of the unit cell V, which we calculate from first principles, as well as the domain wall thickness $2w$ and the domain wall velocity v which we take from experimental literature. Experimental values for $2w$ and v vary strongly throughout the literature, and we therefore estimate them within realistic boundaries. Reported 90° domain wall thicknesses of $BaTiO_3$ range between 2 to 25 nm [37]. Domain wall velocities have been reported up to several times 10^3 m/s for 90° domain wall wedges in $BaTiO_3$ [38,39], as well as several times 10^3 m/s for other domain walls in related ferroelectrics [40]. The ultimate barrier for v is the transverse sound velocity of the material, which in $BaTiO_3$ is 4.4×10^3 m/s [41].

For our first-principles calculations, we use the density functional theory formalism as implemented in the Vienna *ab initio* simulation package (VASP) [42,43]. We use the VASP projector augmented wave (PAW) pseudopotentials with valence electron configurations Ba $5s^2 5p^6 6s^2$, Ti $3d^3 4s^1$, and O $2s^2 2p^4$ and converge the Hellmann-Feynman forces to 0.1 meV/Å. For the 5-atom unit cell, we use a plane-wave energy cutoff of 850 eV, and an $8 \times 8 \times 8$ gamma-centered k-point mesh to sample the Brillouin zone. For the exchange-correlation functional, we choose the Perdew-Burke-Ernzerhof revised for solids (PBEsol) form of the generalized gradient approximation (GGA) [44]. The lattice constants of our fully relaxed tetragonal structure (space group $P4mm$) of $a = 3.983$ and $c = 4.031$ Å with a unit cell volume of $V = 63.9$ Å^3, as well as the calculated ferroelectric polarization of 22.9 μC/cm^2 match reasonably well with experimental values [45]. For a list of the calculated Born effective charges see the Supplemental Material [33].

We show the time evolution of the two amplitudes Q_x and Q_y in Fig. 2(a), and the ionic magnetic moment of the unit cell and its corresponding magnetic field for a domain wall with thickness $2w = 2$ nm and different values of the domain wall velocity v in Fig. 2(d). The quicker the rearrangement, meaning the thinner and faster the domain wall, the larger is the peak magnetic field. For the largest velocity of $v = 4000$ m/s that we show here, the ionic magnetic moment per unit cell reaches $m = 24.7 \times 10^{-6}$ μ_B, which corresponds to an internal magnetic field of $B = 4.5$ μT.

We now extend our calculations to other types of domain walls: to 180° Néel-type domain walls, as were predicted in lead titanate ($PbTiO_3$) [46] and recently observed in lead zirconium titanate (PZT) films [47,48], as well as to polar skyrmions, recently predicted in $BaTiO_3$ [49] and reported in a $PbTiO_3/SrTiO_3$ heterostructure [50], in which electric dipole moments form a spiral structure. We assume pure Néel character for both cases, and consequently the 180° case can straightforwardly be treated as an extension of the 90° case with $n = 2$ in Eq. (5). The center of a moving Néel-type polar skyrmion can be treated as a 360° domain wall

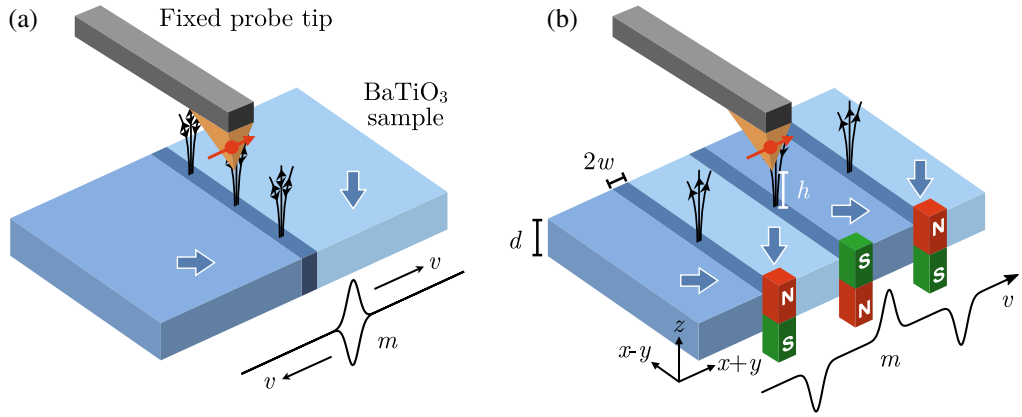

FIG. 3. Proposed experiments to measure the dynamical magnetic field induced by the motion of a ferroelectric domain wall. (a) A time-dependent electric field induces a back-and-forth motion (shivering) of a single domain wall, generating an oscillating magnetic field. (b) A time-dependent electric field in combination with a sawtooth potential provided by the substrate induces unidirectional motion of multiple domain walls as in Ref. [60], generating a magnetic field pulse train with alternating sign.

between domains of the same orientation of polarization with $n = 4$ [51]. In the case of the polar skyrmion, the polarization rotates within a plane perpendicular to the surface and parallel to the direction of domain wall motion, and we have to exchange one of the in-plane ferroelectric components Q_x or Q_y in Eq. (5) for one that is perpendicular to the surface normal Q_z. The magnetic moment according to Eq. (3) then lies in the surface plane, $\mathbf{m} \| y$ or x.

We show the time evolution of the amplitudes Q_x and Q_y for the two cases in Figs. 2(b) and 2(c), and the ionic magnetic moment of the unit cell and its corresponding internal magnetic field in Figs. 2(e) and 2(f). Here, we use a thickness of $2w = 4$ nm for the 180° domain wall and $2w = 8$ nm for the polar skyrmion. By construction, for these wall widths the ionic magnetic moment per unit cell and the internal magnetic field yield the same values as the 90° case, however, with double and four times the full width at half maximum duration of the peak, respectively.

Possible experimental realization.—Nitrogen-vacancy (NV) center defects in diamond have emerged during the past decade as an ultrasensitive detection tool for nanoscale magnetic fields [52–55]. NV centers carry a single electron spin, whose response to changes in the local magnetic field can be observed through their paramagnetic resonance transition [52]. In the field of ferroelectrics, NV center scanning probes have been used to probe the microscopic magnetic texture in multiferroic bismuth ferrite ($BiFeO_3$) [56]. Here, we propose their use in probing the magnetic field at a moving ferroelectric domain wall, exploiting recent improvements in control of ferroelectric domain wall motion, down to the single domain-wall level [57], as compared to their conventional collective motion [58,59].

We show schematic setups of two complementary experiments that could be used to detect the dynamical magnetic field induced by the motion of a ferroelectric domain wall in Fig. 3. In our proposed experiments, a fixed probe using a NV center in a diamond tip is placed above the surface of a $BaTiO_3$ sample. In the first setup, a time-dependent electric field, suitably shielded from the probe tip, induces back-and-forth motion (shivering) of the domain wall, see Fig. 3(a). The magnetic stray field produced by the moving wall will change sign depending on the direction of the domain wall motion, resulting in an oscillatory magnetic signal at the probe tip that is tuned to the resonance frequency of the NV center. In the second setup, motion of multiple domain walls past the tip is induced, see Fig. 3(b). The magnetic moments accompanying each domain wall act as a magnetic pulse train that changes sign as successive domain walls pass the probe tip. If the sizes of the domains are roughly equal, the domain wall velocity is chosen such that the oscillatory magnetic signal caused by the pulse train is tuned to the resonance frequency of the NV center. Unidirectional motion of domain walls has been demonstrated by applying a time-dependent electric field in combination with a sawtooth potential provided by the substrate, which prevents backwards motion over the sawtooth potential edge [60].

We estimate the magnetic stray field at the position of a probe tip located above the surface of $BaTiO_3$ as follows. Tuned to the resonance frequency of the NV center, the dynamical magnetic field of the moving domain wall induces Rabi oscillations. The effective driving field (or Rabi field) B_1 for a thick sample ($d \gg 2w/\beta, h$) and thin moving domain wall ($2w/\beta \ll h$) is given by $B_1 = \gamma n 2\pi\mu_0 f_0/V$, where $\gamma = |\boldsymbol{\gamma}|$ and f_0 is the NV center spin's resonance frequency. (For a detailed derivation, see the Supplemental Material [33].) Our calculations yield a value of $\gamma = 4.8 \times 10^{-41}$ Asm^2. For a NV center near zero bias field, $f_0 \approx 2.87$ GHz, giving a Rabi field of $B_1 \approx 17$ nT for the 90° domain wall configuration of Fig. 3(a) ($n = 1$). For a 180° domain wall, the Rabi field accordingly doubles, $B_1 \approx 34$ nT. These values lie above achievable sensitivities at room temperature and well above

sensitivities projected to be achievable at liquid nitrogen temperatures [61].

Conclusion.—We have identified that moving ferroelectric domain walls have a magnetization resulting from the dynamical multiferroic effect. We predict the magnetic moment accompanying the domain wall motion to reach up to 25 micro μ_B per unit cell, corresponding to the order of several μT. The Rabi field generated by the domain wall of up to 34 nT lies within the range of experimentally achievable sensitivities of NV center magnetometry.

In addition to the 90° and 180° Néel-type domain walls and polar skyrmions studied in this work, our proposed mechanism is generally applicable. We expect, for example, the 71° and 109° domain walls in $BiFeO_3$ or PZT to exhibit strong effects because of their large Born effective charges and domain wall velocities. The mechanism is also valid for Bloch-type domain walls, in which the ferroelectric polarization rotates within a plane perpendicular to the surface and to the direction of domain wall motion, and in this case produces magnetization parallel to the direction of domain wall motion. For pure Ising-type domain walls, in which the polarization reduces to zero at the center of the wall with no perpendicular components, the angular momentum at the domain wall and therefore the effect is zero.

We hope that our proposal sparks experimental efforts to realize the mechanism, adding yet another manipulable degree of freedom to the functionality of domain walls. Experimental success in measuring our proposed phenomenon may result in improved characterization of ferroelectric domain wall motion [35,62], and in detecting possible motion of polar skyrmions and polar vortices [49,50,63].

We are grateful to Pietro Gambardella for useful discussions. This work was supported by the ETH Zurich. Calculations were performed at the Swiss National Supercomputing Centre (CSCS) supported by the project IDs s624, p504. C. L. D. acknowledges funding by the Swiss National Science Foundation under Grant No. 200020-175600 and the NCCR QSIT, and by the European Commission through Grant No. 820394 ASTERIQS. S. T. M. acknowledges funding from the U.S. National Science Foundation, DMR-1410907.

*Present address: Harvard John A. Paulson School of Engineering and Applied Sciences, Harvard University, Cambridge, Massachusetts 02138, USA.

†djuraschek@seas.harvard.edu

[1] P. Paruch, T. Giamarchi, and J.-M. Triscone, Nanoscale studies of domain walls in epitaxial ferroelectric thin films, Top. Appl. Phys. **105**, 339 (2007).

[2] E. K. H. Salje, Domain boundary engineering—recent progress and many open questions, Phase Transitions **86**, 2 (2013).

[3] J. Seidel, L. W. Martin, Q. He, Q. Zhan, Y.-H. Chu, A. Rother, M. Hawkridge, P. Maksymovych, P. Yu, M. Gajek, N. Balke, S. V. Kalinin, S. Gemming, H. Lichte, F. Wang, G. Catalan, J. F. Scott, N. A. Spaldin, J. Orenstein, and R. Ramesh, Conduction at domain walls in oxide multiferroics, Nat. Mater. **8**, 229 (2009).

[4] P. Parucha, T. Giamarchi, T. Tybell, and J.-M. Triscone, Nanoscale studies of domain wall motion in epitaxial ferroelectric thin films, Nat. Mater. **100**, 051608 (2006).

[5] T. Sluka, A. K. Tagantsev, P. Bednyakov, and N. Setter, Free-electron gas at charged domain walls in insulating $BaTiO_3$, Nat. Commun. **4**, 1808 (2013).

[6] J. A. Mundy *et al.*, Atomically engineered ferroic layers yield a room-temperature magnetoelectric multiferroic, Nature (London) **537**, 523 (2016).

[7] D. R. Småbråten, Q. N. Meier, S. H. Skjærvø, K. Inzani, D. Meier, and S. M. Selbach, Charged domain walls in improper ferroelectric hexagonal manganites and gallates, Phys. Rev. Mater. **2**, 114405 (2018).

[8] A. Aird and E. K. H. Salje, Sheet superconductivity in twin walls: Experimental evidence of WO_{3-x}, J. Phys. Condens. Matter **10**, L377 (1998).

[9] S. Van Aert, S. Turner, R. Delville, D. Schryvers, G. Van Tendeloo, and E. K. H. Salje, Direct observation of ferrielectricity at ferroelastic domain boundaries in $CaTiO_3$ by electron microscopy, Adv. Mater. **24**, 523 (2012).

[10] M. Fiebig, Th. Lottermoser, D. Fröhlich, A. V. Goltsev, and R. V. Pisarev, Observation of coupled magnetic and electric domains, Nature (London) **419**, 818 (2002).

[11] T. Lottermoser, T. Lonkai, U. Amann, D. Hohlwein, J. Ihringer, and M. Fiebig, Magnetic phase control by an electric field, Nature (London) **430**, 541 (2004).

[12] A. S. Logginov, G. A. Meshkov, A. V. Nikolaev, E. P. Nikolaeva, A. P. Pyatakov, and A. K. Zvezdin, Room temperature magnetoelectric control of micromagnetic structure in iron garnet films, Appl. Phys. Lett. **93**, 182510 (2008).

[13] Y. Tokunaga, N. Furukawa, H. Sakai, Y. Taguchi, T. Arima, and Y. Tokura, Composite domain walls in a multiferroic perovskite ferrite, Nat. Mater. **8**, 558 (2009).

[14] M. Daraktchiev, G. Catalan, and James F. Scott, Landau theory of domain wall magnetoelectricity, Phys. Rev. B **81**, 224118 (2010).

[15] N. Domingo, S. Farokhipoor, J. Santiso, B. Noheda, and G. Catalan, Domain wall magnetoresistance in $BiFeO_3$ thin films measured by scanning probe microscopy, J. Phys. Condens. Matter **29**, 334003 (2017).

[16] F.-T. Huang, X. Wang, S. M. Griffin, Y. Kumagai, O. Gindele, M.-W. Chu, Y. Horibe, N. A. Spaldin, and S.-W. Cheong, Duality of Topological Defects in Hexagonal Manganites, Phys. Rev. Lett. **113**, 267602 (2014).

[17] V. G. Bar'yakhtar, V. A. L'vov, and D. A. Yablonskii, Inhomogeneous magnetoelectric effect, JETP Lett. **37**, 673 (1983).

[18] A. S. Logginov, G. A. Meshkov, A. V. Nikolaev, and A. P. Pyatakov, Magnetoelectric control of domain walls in a ferrite garnet film, JETP Lett. **86**, 115 (2007).

[19] I. S. Veshchunov, S. V. Mironov, W. Magrini, V. S. Stolyarov, A. N. Rossolenko, V. A. Skidanov, J. B. Trebbia, A. I. Buzdin, Ph Tamarat, and B. Lounis, Direct Evidence of Flexomagnetoelectric Effect Revealed by Single-Molecule Spectroscopy, Phys. Rev. Lett. **115**, 027601 (2015).

[20] G. V. Arzamastseva, A. M. Balbashov, F. V. Lisovskii, E. G. Mansvetova, A. G. Temiryazev, and M. P. Temiryazeva, Properties of epitaxial (210) iron garnet films exhibiting the magnetoelectric effect, J. Exp. Theor. Phys. **120**, 687 (2015).

[21] H. Katsura, N. Nagaosa, and A. V. Balatsky, Spin Current and Magnetoelectric Effect in Noncollinear Magnets, Phys. Rev. Lett. **95**, 057205 (2005).

[22] M. Mostovoy, Ferroelectricity in Spiral Magnets, Phys. Rev. Lett. **96**, 067601 (2006).

[23] R. E. Newnham, J. J. Kramer, W. E. Schulze, and L. E. Cross, Magnetoferroelectricity in Cr_2BeO_4, J. Appl. Phys. **49**, 6088 (1978).

[24] G. A. Smolenskii and I. E. Chupis, Ferroelectromagnets, Sov. Phys. Usp. **25**, 475 (1982).

[25] T. Kimura, T. Goto, H. Shintani, K. Ishizaka, T. Arima, and Y. Tokura, Magnetic control of ferroelectric polarization, Nature (London) **426**, 55 (2003).

[26] D. Khomskii, Classifying multiferroics: Mechanisms and effects, Physics **2**, 20 (2009).

[27] D. M. Juraschek, M. Fechner, A. V. Balatsky, and N. A. Spaldin, Dynamical multiferroicity, Phys. Rev. Mater. **1**, 014401 (2017).

[28] Note that this formula is distinct from the Maxwell-Ampère equation, which predicts a magnetic field curl from a displacement current according to $\nabla \times \mathbf{H} = \partial_t \mathbf{D}$.

[29] K. Dunnett, J.-X. Zhu, N. A. Spaldin, V. Juričić, and A. V. Balatsky, Dynamic Multiferroicity of a Ferroelectric Quantum Critical Point, Phys. Rev. Lett. **122**, 057208 (2019).

[30] D. M. Juraschek and N. A. Spaldin, Orbital magnetic moments of phonons, Phys. Rev. Mater. **3**, 064405 (2019).

[31] A. Barone, F. Esposito, C. J. Magee, and A. C. Scott, Theory and applications of the Sine-Gordon equation, Riv. Nuovo Cimento **1**, 227 (1971).

[32] Y. Ishibashi, Phenomenological theory of domain walls, Ferroelectrics **98**, 193 (1989).

[33] See Supplemental Material at http://link.aps.org/supplemental/10.1103/PhysRevLett.123.127601 for a derivation of the domain wall motion and the stray field estimate, and for a table of the Born effective charges.

[34] M. A. Collins, A. Blumen, J. F. Currie, and J. Ross, Dynamics of domain walls in ferrodistortive materials. I. Theory, Phys. Rev. B **19**, 3630 (1979).

[35] G. Catalan, J. Seidel, R. Ramesh, and J. F. Scott, Domain wall nanoelectronics, Rev. Mod. Phys. **84**, 119 (2012).

[36] E. K. H. Salje, X. Wang, X. Ding, and J. F. Scott, Ultrafast switching in avalanche-driven ferroelectrics by supersonic kink movements, Adv. Funct. Mater. **27**, 1700367 (2017).

[37] J. Hlinka and P. Márton, Phenomenological model of a 90° domain wall in $BaTiO_3$-type ferroelectrics, Phys. Rev. B **74**, 104104 (2006).

[38] H. L. Stadler and P. J. Zachmanidis, Temperature dependence of 180° domain wall velocity in $BaTiO_3$, J. Appl. Phys. **35**, 2895 (1964).

[39] E. Faran and D. Shilo, Twin Motion Faster Than the Speed of Sound, Phys. Rev. Lett. **104**, 155501 (2010).

[40] Q. Meng, M. G. Han, J. Tao, G. Xu, D. O. Welch, and Y. Zhu, Velocity of domain-wall motion during polarization reversal in ferroelectric thin films: Beyond Merz's Law, Phys. Rev. B **91**, 054104 (2015).

[41] W. J. Merz, Switching time in ferroelectric $BaTiO_3$ and its dependence on crystal thickness, J. Appl. Phys. **27**, 938 (1956).

[42] G. Kresse and J. Furthmüller, Efficiency of ab-initio total energy calculations for metals and semiconductors using a plane-wave basis set, Comput. Mater. Sci. **6**, 15 (1996).

[43] G. Kresse and J. Furthmüller, Efficient iterative schemes for ab initio total-energy calculations using a plane-wave basis set, Phys. Rev. B **54**, 11169 (1996).

[44] G. I. Csonka, J. P. Perdew, A. Ruzsinszky, P. H. T. Philipsen, S. Lebègue, J. Paier, O. A. Vydrov, and J. G. Ángyán, Assessing the performance of recent density functionals for bulk solids, Phys. Rev. B **79**, 155107 (2009).

[45] K. J. Choi, M. Biegalski, Y. L. Li, A. Sharan, J. Schubert, R. Uecker, P. Reiche, Y. B. Chen, X. Q. Pan, V. Gopalan, L.-Q. Chen, D. G. Schlom, and C. B. Eom, Enhancement of ferroelectricity in strained $BaTiO_3$ thin films, Science **306**, 1005 (2004).

[46] D. Lee, R. K. Behera, P. Wu, H. Xu, Y. L. Li, S. B. Sinnott, S. R. Phillpot, L. Q. Chen, and V. Gopalan, Mixed Bloch-Néel-Ising character of 180° ferroelectric domain walls, Phys. Rev. B **80**, 060102(R) (2009).

[47] G. De Luca, M. D. Rossell, J. Schaab, N. Viart, M. Fiebig, and M. Trassin, Domain wall architecture in tetragonal ferroelectric thin films, Adv. Mater. **29**, 1605145 (2017).

[48] S. Cherifi-Hertel, H. Bulou, R. Hertel, G. Taupier, K. D. H. Dorkenoo, C. Andreas, J. Guyonnet, I. Gaponenko, K. Gallo, and P. Paruch, Non-Ising and chiral ferroelectric domain walls revealed by nonlinear optical microscopy, Nat. Commun. **8**, 15768 (2017).

[49] Y. Nahas, S. Prokhorenko, L. Louis, Z. Gui, I. Kornev, and L. Bellaiche, Discovery of stable skyrmionic state in ferroelectric nanocomposites, Nat. Commun. **6**, 8542 (2015).

[50] S. Das *et al.*, Observation of room-temperature polar skyrmions, Nature (London) **568**, 368 (2019).

[51] Note that the skyrmions in the reported case of a $PbTiO_3/SrTiO_3$ heterostructure are Bloch type.

[52] C. L. Degen, Scanning magnetic field microscope with a diamond single-spin sensor, Appl. Phys. Lett. **92**, 243111 (2008).

[53] J. R. Maze, P. L. Stanwix, J. S. Hodges, S. Hong, J. M. Taylor, P. Cappellaro, L. Jiang, M. V. Gurudev Dutt, E. Togan, A. S. Zibrov, A. Yacoby, R. L. Walsworth, and M. D. Lukin, Nanoscale magnetic sensing with an individual electronic spin in diamond, Nature (London) **455**, 644 (2008).

[54] J. M. Taylor, P. Cappellaro, L. Childress, L. Jiang, D. Budker, P. R. Hemmer, A. Yacoby, R. Walsworth, and M. D. Lukin, High-sensitivity diamond magnetometer with nanoscale resolution, Nat. Phys. **4**, 810 (2008).

[55] F. Casola, T. van der Sar, and A. Yacoby, Probing condensed matter physics with magnetometry based on nitrogen-vacancy centres in diamond, Nat. Rev. Mater. **3**, 17088 (2018).

[56] I. Gross, W. Akhtar, V. Garcia, L. J. Martínez, S. Chouaieb, K. Garcia, C. Carrétéro, A. Barthélémy, P. Appel, P. Maletinsky, J. V. Kim, J. Y. Chauleau, N. Jaouen, M. Viret, M. Bibes, S. Fusil, and V. Jacques, Real-space imaging of

non-collinear antiferromagnetic order with a single-spin magnetometer, Nature (London) **549**, 252 (2017).

[57] L. J. McGilly, P. Yudin, L. Feigl, A. K. Tagantsev, and N. Setter, Controlling domain wall motion in ferroelectric thin films, Nat. Nanotechnol. **10**, 145 (2015).

[58] P. Bintachitt, S. Jesse, D. Damjanovic, Y. Han, I. M. Reaney, S. Trolier-McKinstry, and S. V. Kalinin, Collective dynamics underpins Rayleigh behavior in disordered polycrystalline ferroelectrics, Proc. Natl. Acad. Sci. U.S.A. **107**, 7219 (2010).

[59] D. M. Marincel, H. R. Zhang, J. Britson, A. Belianinov, S. Jesse, S. V. Kalinin, L. Q. Chen, W. M. Rainforth, I. M. Reaney, C. A. Randall, and S. Trolier-McKinstry, Domain pinning near a single-grain boundary in tetragonal and rhombohedral lead zirconate titanate films, Phys. Rev. B **91**, 134113 (2015).

[60] J. R. Whyte and J. M. Gregg, A diode for ferroelectric domain-wall motion, Nat. Commun. **6**, 7361 (2015).

[61] T. Joas, A. M. Waeber, G. Braunbeck, and F. Reinhard, Quantum sensing of weak radio-frequency signals by pulsed Mollow absorption spectroscopy, Nat. Commun. **8**, 964 (2017).

[62] P. Sharma, Q. Zhang, D. Sando, C. H. Lei, Y. Liu, Ji. Li, V. Nagarajan, and J. Seidel, Nonvolatile ferroelectric domain wall memory, Sci. Adv. **3**, e1700512 (2017).

[63] A. K. Yadav, C. T. Nelson, S. L. Hsu, Z. Hong, J. D. Clarkson, C. M. Schlepuëtz, A. R. Damodaran, P. Shafer, E. Arenholz, L. R. Dedon, D. Chen, A. Vishwanath, A. M. Minor, L. Q. Chen, J. F. Scott, L. W. Martin, and R. Ramesh, Observation of polar vortices in oxide superlattices, Nature (London) **530**, 198 (2016).